# A Low-Noise and Wide Dynamic Range 15 MHz CMOS Receiver for Pulsed Time-of-Flight Laser Ranging

Sami Kurtti [ID], Aram Baharmast [ID], *Graduate Student Member, IEEE*, Jussi-Pekka Jansson [ID], and Juha Kostamovaara [ID], *Life Senior Member, IEEE*

Abstract—**A laser radar receiver channel targeted at pulsed time-of-flight laser radar applications using 5ns…20ns laser pulses at the 1550nm wavelength region has been designed. The receiver includes a transimpedance preamplifier, post-amplifiers and analog output buffer and has a bandwidth of 15MHz and input reduced total equivalent current noise of ∼3nArms without the contribution of the APD noise. The receiver supports both the single shot and transient recording operation modes. By utilizing the time domain compensation methods, the single shot timing walk is at the level of +/−100ps within a wide dynamic range of 1: 36 000 of the received echo amplitudes. It is demonstrated that the designed receiver allows the pulsed time-of-flight measurement in the single shot mode to non-cooperative targets up to distances of several hundreds of meters with a laser pulse power of 4 W and receiver aperture of 20mm.**

Index Terms—**Laser radar, lidar, optical receiver, timing discrimination.**
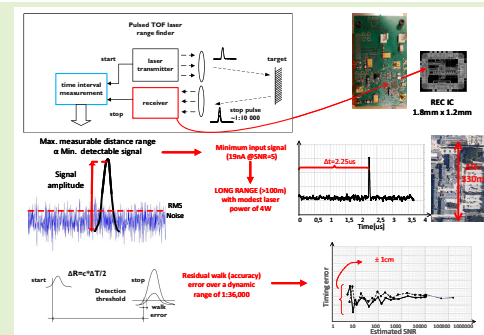
I. INTRODUCTION

LASER radars are used widely in a variety of distance measurement applications. The advantage of a radar working at optical wavelengths is good spatial resolution, which is due to the easy collimation of optical beams with appropriate optics. As is well-known, collimation of the beam is much more challenging at radio frequencies, due to the much longer wavelength of the electromagnetic signal. In applications requiring high measurement speed, e.g. in the ms range, and long distances (>100m), pulsed time-of-flight (TOF) laser range finding techniques are typically used. These techniques are based on measurement of the flight time of a short laser pulse to the target and back to the receiver. With ns-range pulses a relatively high precision of a few cm can be achieved even with a single laser shot [1]–[5].

Techniques based on single photon detector receivers have attracted much attention recently, especially in pulsed

time-of-flight lidar projects aimed at developing solid-state 2-D or 3-D range imaging devices [6]–[10]. Autonomous, driverless cars are one example of an application that obviously calls for mid or long-range high-speed environment-sensing techniques, and other potential applications of growing importance are robotics (environment perception) and autonomous or semiautonomous control of machines (excavators, bulldozers etc.) and small vehicle guidance (e.g. Unmanned Aerial Vehicles (UAVs)). Single-photon detectors (SPADs) can be realized in standard CMOS technologies together with other necessary electronics, i.e. time-to-digital converters (TDCs), even as dense arrays [11]. These are sensitive and require virtually no analogue amplifiers, so that in principle high system level integration is possible. On the other hand, a digital breakdown-based SPAD detector cannot distinguish between a random photon produced by the background illumination and a signal photon from the target. Thus, in applications where the background illumination level is high, e.g. out of doors, the random background will radically lower the signal-to-noise level of the measurement and may even block the receiver on account of the finite dead-time of the detector [12], [10], [13], [4]. This places serious limitations on these techniques in the rapidly widening application field of 3D range imaging.

For a pulsed TOF lidar receiver based on linear optical detection techniques, i.e. using an avalanche photon
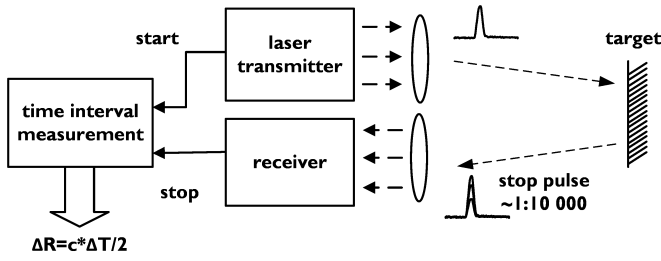
Fig. 1. Block diagram of a typical pulsed time-of-flight laser radar.

detector (APD) and a sensitive analogue receiver channel, the background illumination is just one of the noise sources among many others, and thus its effect on the receiver performance is typically less severe. For this reason, a pulsed TOF lidar that uses a linear receiver and a micro-mechanical scanner, for example, to enhance the per-pulse sensitivity is an interesting alternative approach for 3-D range imaging. A solid-state focal plane scanning architecture is also possible in principle, but it suffers from the limited availability of dense linear mode 2-D detector arrays, and also from sensitivity issues [14].

In linear mode pulsed, TOF lidars, short laser pulses of length 3…5ns are typically used, see Fig. 1 for a typical block diagram of pulsed time-of-flight laser radar. The receiver channel bandwidth is often in the 100MHz…200MHz range in order to preserve the pulse shape in the detection and to allow high timing accuracy within a wide dynamic range of echo pulse amplitudes [15]–[18]. It is well known from the theory of optical communications, however, that the bandwidth maximizing the signal-to-noise ratio (SNR) in the detection for pulses of this kind is achieved with a much lower bandwidth [19], [20]. In optical telecommunications the lowering of the bandwidth is subject to a trade-off with the resulting inter-symbol interference (ISI) [21], [22], but in laser radars the ISI is not an issue due to the much lower pulsing rate, typically 10kHz…1MHz. The need to be able to detect multiple echoes and reduce the timing walk error may still favour the use of short laser pulses and a higher bandwidth, but if distances of several hundreds of metres to non-cooperative targets are aimed at with laser diodes having a pulse power in the 10W region, the receiver sensitivity should be optimized from the SNR point-of-view, as discussed in detail in later sections. The resulting larger intrinsic timing walk error can be minimized by measuring the time parameters (pulse width and/or rise time) from the detected echo pulse, as recently suggested in [17], [23]–[25], for example.

This paper presents a design for a CMOS laser radar receiver channel which is optimized in terms of high sensitivity. The optimization is based on using a relatively low receiver bandwidth (∼15MHz) compared to conventional designs (∼150MHz). In order to avoid the deterioration of the timing accuracy due to the lower bandwidth, time-domain timing walk error compensation techniques are used. In particular, the width of the received laser pulse and the rise time of its leading edge between two present threshold levels are also measured simultaneously with the time position of the received laser echo pulse with respect to the start pulse (i.e. the

triggering of the laser diode transmitter). These measurements allow one to estimate the timing walk error and compensate it for accordingly within a wide dynamic range of input echo amplitudes, as is experimentally demonstrated.

The receiver channel is intended for use with laser pulses within the width range of ∼5ns…20ns, so that it can be used with many kinds of pulsed laser sources, e.g. with laser diode and solid-state laser-based transmitters. In addition to the use of time-domain timing walk error compensation techniques, another distinct feature of the receiver developed here is that it can work in dual modes: a high-SNR mode in which the receiver allows single shot detection of echo pulses exceeding the present threshold and the direct measurement of the time interval between the emitted laser shot and the received echo pulse, and a low-SNR mode in which the output of the receiver can be continuously sampled with a comparator. The averaging of successively recorded output transients allows for echo pulse detection even with a signal-to-noise ratio (SNR) of <1, albeit at the cost of increased measurement time. The present receiver channel is characterized by the use of a 4W laser diode transmitter working at the eye-safe 1550nm wavelength region and achieves a single-shot measurement range of several hundred metres to non-cooperative targets with a ∼20mm receiver aperture, which makes it interesting for autonomous driving applications, for example.

This paper continues by setting out the operation principle and a brief analysis of the SNR and other relevant performance parameters achievable in a pulsed time-of-flight laser radar working in the approx. 1550nm wavelength region in Section 2. The design principles of the receiver channel developed here are then described in Section 3, and Section 4 gives details of the circuit blocks of the receiver chip and the results of a characterization of the chip, together with some system-level results. Finally, the conclusions and a summary of the work are presented in Section 5.

II. LASER RADAR RECEIVER PERFORMANCE
A. The Signal-to-Noise Ratio in Laser Ranging

Assuming a non-cooperative (Lambertian) target, the current signal produced by the optical detector (here an avalanche photo diode, APD) as a function of the distance can be calculated using the well-known radar equation (1). Vignetting has been neglected in this case since we are mainly interested in the SNR at long distances (i.e. at the limit of the sensitivity of the device), where vignetting is not important [27]. It is also assumed that the target completely fills the transmitter beam.

$$
\begin{aligned}
i_{APD}(R) &= M_{APD} \cdot i_{sig}(R) \\
&= \frac{P_{tr} \cdot \tau_{opt} \cdot \rho_{t\,arget} \cdot A_{rec}}{\pi \cdot R^2} \cdot M_{APD} \cdot R_{APD} \quad (1)
\end{aligned}
$$

In this equation $i_{APD}(R)$ is the current produced by the APD and the other parameters are as given in Table I. With the typical system parameter values indicated in Table I and using an avalanche detector as the optical receiver in a system working in the wavelength of 1550nm, the signal current from a distance (R) of 200m, for example, is ∼30nA. This means that the input-referred equivalent rms current noise of the receiver should be only a few nanoamperes, in order to

TABLE I
PARAMETERS OF THE LASER RADAR SYSTEM

Symbol	Quantity	Unit
P_{tr}	laser pulse power	10 W
τ_{opt}	transmission of optics	0.5
$\rho_{targert}$	target reflectivity	0.3
A_{rec}	receiver aperture	$3 \cdot 10^{-4}$ m^2
R_{APD}	intrinsic responsivity of the APD detector	0.9 A/W @1550nm
M_{APD}	Gain of the APD	10

achieve the SNR of 5…10 which is needed for reliable single shot detection of the laser pulse echo. This is a markedly lower value than is typically available in wide-band receivers (50…100nArms, as in [15], [17], and [25], for example), and thus optimization of the receiver with respect to noise is needed [26].

The noise in the detection process is produced by the electronic noise of the receiver channel and the shot noise of the dark current of the APD, the dc current induced by the background radiation and the signal current, as indicated in (2)

$$i_{noise,in}^2 = 2e(R_{APD} \cdot P_{BG} + I_{dark} + R_{APD} \cdot \bar{i}_{sig})$$
$$\cdot M_{APD}^2 \cdot F_M \cdot BW + i_{eqvn,amp}^2. \quad (2)$$

In this equation $i_{noise,in}$ is the total input current noise at the input to the receiver channel, e the charge of the electron, P_{BG} the background radiation power falling on the detective surface of the APD, I_{dark} the primary dark current of the APD, M_{APD} the gain in the APD, F_M the excess noise factor of the APD due to statistical fluctuation in the avalanche gain process and BW the noise bandwidth of the receiver channel. The term $i_{noise,in}$ indicates the input-referred equivalent current noise of the receiver channel. The value of this noise depends on the total input capacitance and design details of the preamplifier, and also on the bandwidth of the receiver [20].

Due to the excess noise factor F_M ($\sim M^x$, $x \sim 0.5$), the gain in the APD typically has an optimum value at which the SNR (the ratio of the peak value of the signal current to the total rms noise current, $i_{APD}/i_{noise,in}$) is at its maximum. This operation point is achieved when the total of the other noise sources is approximately equal to the noise of the receiver electronics.

B. Timing Jitter and Timing Walk Error

The minimum SNR limits the sensitivity of detection, i.e. the probability of detection and the false alarm triggering rate, as discussed in detail elsewhere, e.g. in [3]. This will also affect the random timing jitter in the detection of the echo pulse. Assuming that a constant threshold is used in the timing detection, the jitter will be roughly proportional to the ratio of the rise time of the echo pulse to the SNR, see Fig. 2 and (3) [2].

$$\sigma_{time} \approx \frac{\sigma_{noise}}{dv_{sign}/dt} \simeq \frac{t_{rise}}{SNR} \quad (3)$$

In Equation (3), σ_{time} is the sigma value of the timing jitter, σ_{noise} is the sigma value of the voltage noise at the input to the
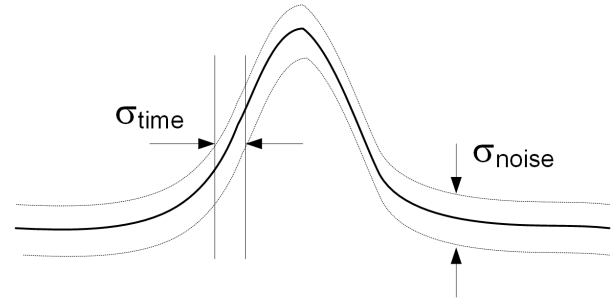

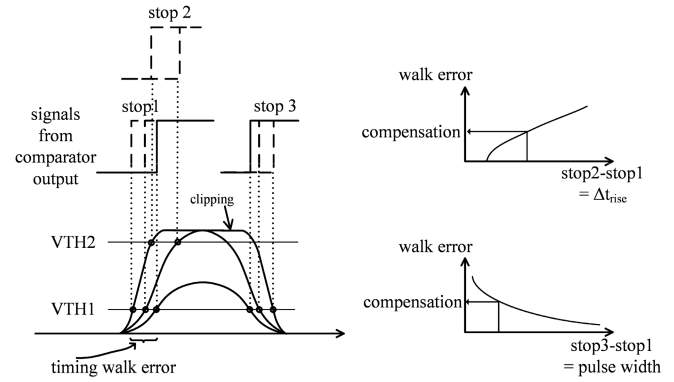Fig. 2. Jitter of the timing pulse at the detection threshold level.

Fig. 3. Timing walk error and its compensation using the measured pulse width and/or rise time between two thresholds.

timing detector, and the denominator indicates the slew-rate of the timing signal at the detection threshold. Thus, in principle, the use of a wide bandwidth in the transmitter/receiver would help to improve the timing jitter in the detection, but only at the expense of lower sensitivity (and thus of a smaller maximum range, for example). Consequently, if the rise time of the timing pulse is ~1ns, the single shot timing jitter at an SNR of 10 will be ~100ps, which corresponds to a distance uncertainty of 1.5cm. It is important to note, however, that the jitters of a low and a wide bandwidth receiver at the same signal current level will not differ markedly, due to the fact that although the rise time is longer with the low bandwidth receiver, the SNR will be correspondingly higher.

Another important source of error is the systemic timing walk error, which is induced due to the varying amplitude of the received echo signal. The echo pulse amplitude depends on the measurement distance and the orientation and reflectivity of the target, see (1), and the variation in these may amount to 1:10 000…100 000 depending on the range and the reflection properties of the objects. In traffic applications, for example, a painted metal surface, e.g. that of a car, can in some cases give a very strong mirror-like reflection, while in other cases the same target can be covered in mud, resulting in a very low reflection. With the typical leading-edge timing discrimination based on a constant threshold level, see Fig. 3, this amplitude variation will introduce a timing error which is proportional to the slew-rate of the timing pulse. One part of this error is produced simply by the geometrical variation in the timing point, whereas part of it is produced due to variation in the group delay in the receiver channel in response to the varying slew-rate of the analogue timing signal [28], [29].

A typical value for the total timing walk error of a wide band (~150MHz) laser radar receiver is ~2ns [23]. For a receiver with lower bandwidth, e.g. for 15MHz, the intrinsic timing walk error would be correspondingly larger, i.e. ~20ns.

As is seen in Fig. 3, timing pulses of higher amplitude are also wider at the detection threshold, and thus it is obviously possible to compensate for the timing walk error by measuring the width of the timing pulse (and/or its rise time) [17], [23], [25]. The use of this method typically necessitates a separate calibration measurement in which the relation between the measured time-domain parameter (e.g. the width of the timing pulse) and the timing walk error is determined.

Another technique for producing a timing mark with a low timing error is to generate a bipolar signal from the unipolar detector current pulse already at the input of the receiver channel. The zero-crossing of this signal will in principle not be dependent on the amplitude of the echo pulse. Thus, by designing the receiver electronics so that they would rapidly recover from the clipping mode that is inevitable for a signal exceeding its linear range, a low timing error can in principle be achieved over a wide dynamic range simply by using the zero-crossing as the timing mark [18].

In nuclear electronics, constant fraction discrimination techniques (CFD) are typically used to avoid the timing walk. They work well however only within the linear range of the signal and are thus not easily adapted to a laser radar receiver where the linear dynamic range of the preamplifier is typically ~1:100 while the echo amplitude range to be covered is typically >1: 10 000.

C. Sensitivity Optimization

Based on the above discussion, we know that for a successful design of a receiver for a pulsed TOF laser radar it is important to simultaneously optimize the sensitivity of the receiver, i.e. maximize the SNR, and to achieve low enough timing walk error within the dynamic range of the echo amplitudes. One obvious possibility to increase the sensitivity of the receiver is to increase the energy of the optical pulse (i.e. by increasing its amplitude and length) and then reducing the f_{-3dB} bandwidth of the receiver correspondingly to match the receiver with the used laser pulse properties. As already discussed above, this comes however only at the cost of increased intrinsic timing walk error, which has to be compensated for. The typical pulse/BW parameters used in pulsed TOF laser radars are ~3ns/~150MHz. In this work, the nominal laser pulse length was however selected to be 10ns (in practise a laser pulse with a length in the range of 5ns…20ns could well be used) and the bandwidth of the receiver is optimized with regard to this selection to maximize sensitivity of the receiver. The increased intrinsic timing walk error is compensated for by the combination of the time-domain compensation techniques as suggested in Section II.B and demonstrated in more details in the experimental part of the work (Section IV).

In this section, it is shown that for the selected laser pulse length and APD parameters in the transimpedance preamplifier configuration there is an optimum bandwidth from the maximum SNR point of view. The analysis is carried
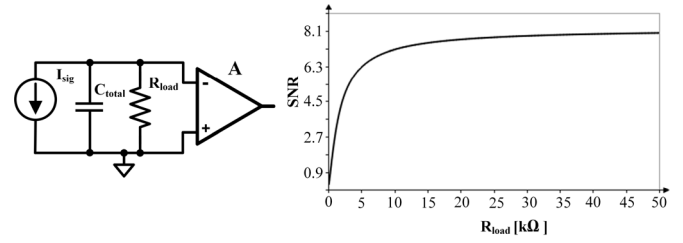

Fig. 4. A high-impedance receiver and its SNR as a function of the load resistance, $i_{s,pr}$ = 10nA (M = 10), C_{total} = 3.5pF, Δt_{pulse} = 10ns. Only the thermal noise of R_{load} is considered.

out by fixing the input capacitance (dominated typically by the APD capacitance) and feedback resistance (close to the transimpedance limit [30]) and using the gain A_{OP} of the feed-forward voltage amplifier as the means to set the bandwidth of the receiver.

In optical receivers the current signal received from the photo detector is usually converted to a voltage signal at the input to the receiver. A straight-forward circuit technique for doing this would be to use a high-impedance receiver consisting of a resistor and a voltage mode amplifier chain. This configuration is shown in Fig. 4. The input capacitance, which is the total sum of the detector, preamplifier, bonding and input pad together with stray capacitances, is also shown. For pulsed TOF laser radars working at 1550nm, the high-power pulse mode laser diodes typically have a relatively wide active stripe width of ~100μm, which necessitates the use of optical detectors with an active region width of the same size or larger. Thus, the resulting input capacitance is typically of the order of a few picofarads.

The load resistance R_{load} in this configuration should obviously be as high as possible (integrating mode) in order to achieve the maximum SNR. This SNR is nevertheless limited by the kT/C noise which is a serious limitation at high input capacitances. For example, assuming a rectangular laser pulse length of 10ns and a total input capacitance of 3.5pF, the maximum SNR according to (4) and the simulation in Fig. 4 at a primary signal current of 10nA (M = 10) would only be around 8, even when neglecting all other sources of noise than the thermal noise of the load resistor. The SNR is defined here as the ratio of the peak signal value over the rms value of the noise signal.

$$SNR_{\max} \simeq \frac{\frac{i_{s,pr} \cdot M \cdot \Delta t_{pulse}}{C_{total}}}{\sqrt{\frac{kT}{C_{total}}}} = \frac{i_{s,pr} \cdot M \cdot \Delta t_{pulse}}{\sqrt{kT \cdot C_{total}}}$$

$$= \frac{10 \cdot 10^{-9} \cdot 10 \cdot 10 \cdot 10^{-9}}{\sqrt{4.05 \cdot 10^{-21} \cdot 3.5 \cdot 10^{-12}}} \approx 8 \qquad (4)$$

Let's next consider the sensitivity that can be achieved with the transimpedance amplifier configuration as shown in Fig. 5.

Assuming first for simplicity an infinite bandwidth for the feed-forward voltage amplifier, the transimpedance can be given as

$$Z_T(s) = \frac{R_{fb} \cdot A_{OP}}{1 + A_{OP}} \times \frac{1}{1 + \frac{s}{\left(R_{fb} \cdot C_{total}/A_{OP}\right)}}. \qquad (5)$$
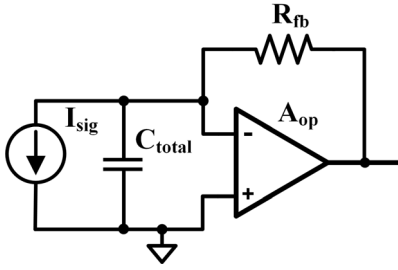
Fig. 5. The transimpedance configuration.

In Equation (5), A_{OP} is the gain of the feed-forward voltage amplifier and R_{fb} is feedback resistor. Since the transimpedance within the signal band is $\sim R_{fb}$ and the bandwidth is $A_{OP}/(R_{fb}C_{total})$, the SNR in the case in which R_{fb} noise predominates can be approximated in the form

$$SNR(A_{OP}) \simeq \frac{i_{sig} \cdot M \cdot R_{fb} \cdot \left(1 - e^{\frac{-\Delta t_{pulse}}{\frac{R_{fb}}{A_{OP}} \cdot C_{total}}}\right)}{\sqrt{A_{OP} \cdot kT / C_{total}}}. \quad (6)$$

Again, the higher the resistance of the feedback resistor R_{fb} is, the better is the SNR. The maximum value for this resistance for a given bandwidth (BW) and device technology as characterized by the unity current gain transition frequency f_T is set by the so-called "transimpedance limit", according to (7):

$$R_{fb,max} \approx \frac{f_T}{2\pi \cdot C_{total} \cdot f_{3dB}^2}, \quad (7)$$

where f_{3dB} is the desired 3-dB bandwidth [30]. Assuming the use of $0.35\mu m$ CMOS technology, for which the f_T for large input transistors (W/L$\sim$3000) could well be $\sim$1.2GHz, and the intended bandwidth $\sim$15MHz, $R_{fb,max}$ can be evaluated to be roughly 250kΩ.

The SNR determined on the basis of (6) (in which R_{fb} = 250kΩ was used here) peaks at the open loop gain value of A_{OP} = 100 and amounts to $\sim$50, which is markedly higher than with a high-impedance front end. Thus, the optimum bandwidth of the receiver at this point in the operation would from the SNR point of view be $\sim$18MHz for a pulse of width 10ns, i.e. $BW_{opt} \sim 0.2/\Delta T$.

In a more realistic design case consideration should also be given to other noise sources (i.e. noises of the amplifier, AP diode and signal) and to the limited bandwidth of the feed-forward voltage amplifier. Fig. 6 shows the calculated dependence of the SNR on the open loop gain in the preamplifier in a situation where all the parameters are as above and in addition the APD is assumed to have a primary dark current of 5nA and an excess noise factor $F_M = 10^{0.55}$. The primary signal current is assumed to be 10nA, and the equivalent spectral input voltage noise of the preamplifier to be $\sim$1nV/$\sqrt{Hz}$. The open loop response of the preamplifier is assumed to have three poles located at a frequency of $\sim$3 $\times$ BW_{ZT} (equivalent input noise and pole location roughly mimicking the 3-stage preamplifier designed here). The dotted curve shows the calculated approximation for the SNR of
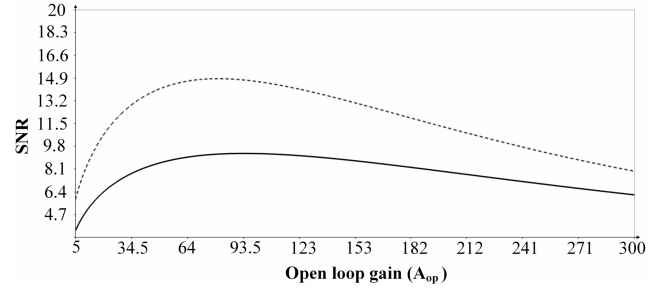

Fig. 6. SNR as a function of the preamplifier open loop gain; dotted curve: without signal shot noise, solid curve: signal shot noise included.
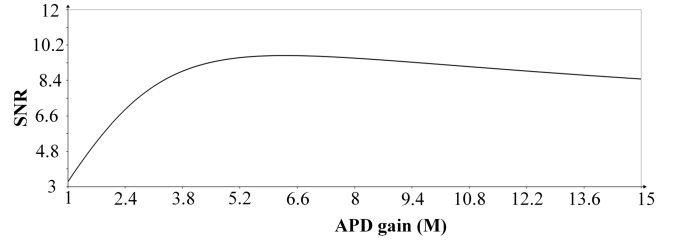

Fig. 7. SNR as a function of the APD gain M (A_{OP} set to 80).

the receiver without the contribution of the signal shot noise. The solid curve shows the total SNR with the signal shot noise included. As can be seen, the signal shot noise has an appreciable lowering effect on the SNR. In general, additional noise sources tend to lower the optimum receiver bandwidth, but the effect of the signal shot noise obviously smooths the dependence of the SNR on the bandwidth of the receiver. The optimum preamplifier open loop gain is seen to be $\sim$80, and thus the optimum preamplifier bandwidth for a laser pulse with a width of 10ns is $\sim$15MHz with the given total input capacitance.

As already pointed out above, in the context of APD design an optimum gain can exist for the APD. In this particular design case, the optimum gain is $M_{opt} \sim$6, as indicated by the calculation shown in Fig. 7, which shows the calculated SNR as a function of the APD gain (preamplifier open loop gain set to 80). The dependence of the SNR on the APD gain is not very strong, however, especially above the optimum operation point.

It can be concluded from the above analysis that from the SNR optimization point of view the optimum bandwidth of a pulsed TOF lidar receiver is typically around $(0.15...0.2)/\Delta t_{pulse}$. Also, the APD dark current and signal shot noise values may make a substantial contribution to the overall SNR in low-noise designs and should therefore be considered carefully.

III. RECEIVER DESIGN

A. Receiver Architecture and Circuit-Level Design

A block diagram of the laser radar receiver is shown in Fig. 8. Its functional blocks are the low-noise preamplifier, post-amplifiers and a continuous-time (not clocked) comparator with an output that can be sampled for the transient recording. Single shot echoes are available from the analogue output buffer for timing discrimination and time interval
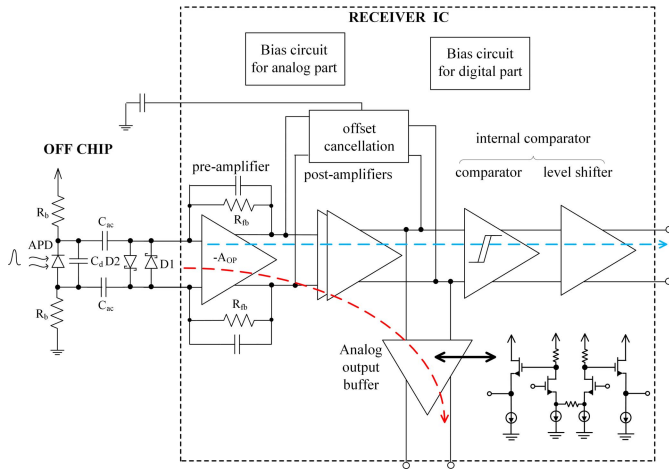
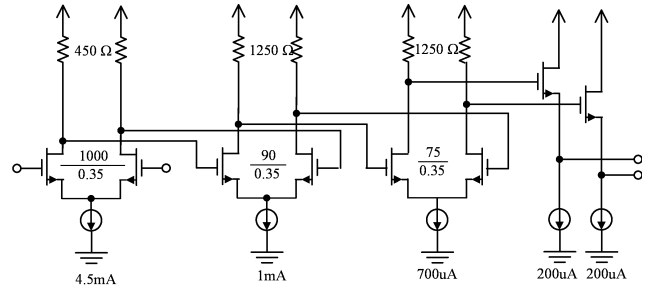Fig. 8. Block diagram of the laser radar receiver circuit.
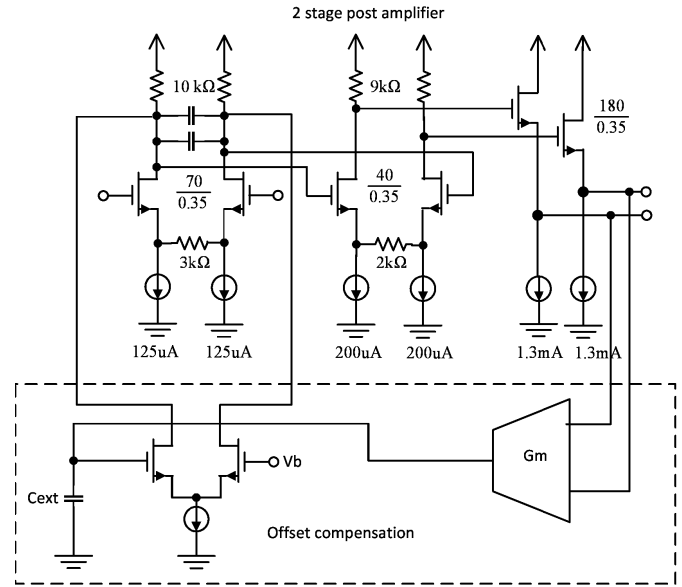

Fig. 9. The core amplifier of the transimpedance stage.

Fig. 10. The post amplifier circuitry including offset cancellation. The nominal gain of the post amplifier is 7.

measurement. The avalanche photodiode (IAG-200 by Laser Components) is ac-coupled to the transimpedance amplifier input and resistively biased to the bias voltage (∼50V).

The important design features include minimization of noise in the receiver by setting its bandwidth according to the principles presented in Section 2. The minimization of electronic noise in transimpedance preamplifiers is well covered in the literature and the known principles were applied here when designing the preamplifier, see [20], [30] and references therein.

It is often the front end of the receiver channel that limits its performance of, and this is the most critical block from a design point of view due to the partly conflicting requirements, such as low noise, stability and wide linear range. In the present design R_{fb} was set to 270kΩ. The transistor-level structure of the fully differential core amplifier (A_{OP}) in the transimpedance amplifier, as shown in Fig. 9, comprises three common source amplifier stages with resistive loads in order to achieve adequate internal gain in the core amplifier (A_{OP}) for the targeted bandwidth of ∼15MHz.

The predominant sources of noise in the CMOS transimpedance preamplifier, shown in Fig. 9, are the thermal noise feedback resistors and the input-referred voltage noise of the core amplifier [20]

$$i_{n,in}(\omega) \approx \frac{4kT}{R_{fb}} + \frac{8}{3} \cdot \frac{4kT}{g_m} \cdot (\omega \cdot C_{total})^2. \tag{8}$$

The second term in (8) is related to the input stage of the preamplifier and causes the noise to peak at higher frequencies, although this is filtered by the non-dominant poles of the preamplifier.

The stability of the preamplifier has to be considered separately, especially in cases where the core amplifier has several gain stages and thus high frequency poles. The dominant pole of the open loop frequency response is located at the input node, while the non-dominant poles are the poles of the internal stages of the core amplifier. To improve stability, a compensation capacitor is placed in parallel with the feedback resistor, as shown in Fig. 8.

The post-amplifier, consisting of two voltage stages, and the offset cancellation loop are shown in Fig. 10. The gain

in the post-amplifier needs to be high enough for the timing comparator to reliably detect the optical input signal at the limit of the sensitivity of the receiver. To enhance noise filtering at the post-amplifier stage, extra capacitors are also placed at the output from the first post-amplifier stage.

An offset cancellation circuit is added to the post-amplifier to minimize the offset created by mismatches, e.g. in the input transistors and feedback resistors of the preamplifier. The offset cancellation circuitry takes the post-amplifier output to the Gm block, which integrates an error voltage at its output. This voltage drives a differential pair to compensate for the voltage differences and correspondingly reduce the offset voltage. The lower frequency limit of the offset compensation loop was set to be 20Hz.

The analogue output buffer, shown in Fig. 8, is designed to be sufficiently fast, wide and linear that it does not distort the amplifier channel output. Analogue buffer outputs are then taken from the source follower stage, resulting in a buffer gain of about ∼1. As a result, the total gain from the input to the analogue output (i.e. in the transimpedance, post-amplifier and analogue output stages) is about 3.5MΩ (500k × 7 × 1).

Since the timing comparator provides positive and negative samples (or zeros and ones) with equal probability only if the random noise at its input (with the embedded weak echo pulse) is markedly larger that the comparator offset voltage, the total
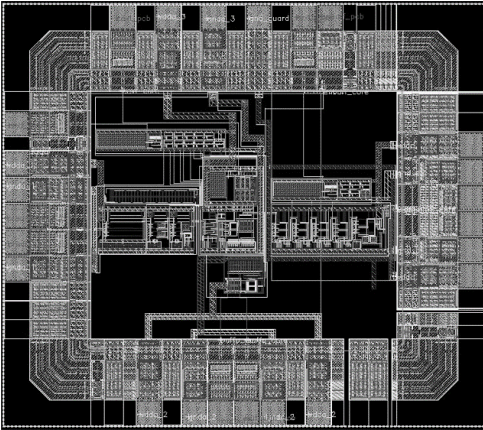
Fig. 11. Layout of the pulsed TOF lidar receiver designed here.

Fig. 12. Configuration for measurement of the frequency response.

gain of the receiver (effective transimpedance) was set so that the receiver noise level at the input to the timing comparator was ~5-10mV. The channel offset, the offset introduced by the preamplifier and post-amplifiers, was cancelled out with an on-chip feedback circuit. Thus, the remaining offset in the detection was mostly that of the comparator only. Differential signal processing was utilized throughout the design to suppress the effect of common mode disturbances.

The comparator output was intended to be sampled into a shift register at a rate of 100MS/s, enabling a record with a length of 81.92μs (or 12.2km in distance), for example, to be saved for a single laser shot with a register length of 2^{13} bits. Successive transients could then be averaged to the extent desired, and other types of digital filtering could also be applied, e.g. in order to set the receiver bandwidth accurately. The digital functionalities, including the PC interface, were realized with a separate FPGA board.

The analogue receiver channel was realized in a standard 0.35μm CMOS technology with a 3.3V supply voltage. The size of the chip was 1.8mm $\times$ 1.2mm including the bonding pads, and the key performance parameters were confirmed with simulations in all technology corners and within a temperature range of $-40 \ldots +80°C$. The layout of the receiver, which has a static power consumption of ~60mW, is shown in Fig. 11.

IV. RECEIVER PERFORMANCE

The important performance parameters from a laser radar point of view are the frequency response, the total gain (transimpedance) and the receiver noise, which determines the sensitivity of the receiver (maximum measurement range).

A. Frequency Response

As explained above, the laser radar receiver was designed for laser pulses with a width of ~5…20ns, so that the bandwidth of the channel was set to ~15MHz in order to maximize its sensitivity for 10ns pulses. It should be noted that in the transient recording mode the final bandwidth can easily be lowered by means of digital post-processing of the averaged transient record.

The frequency response of the receiver was measured with the configuration shown in Fig. 12, in which a differential
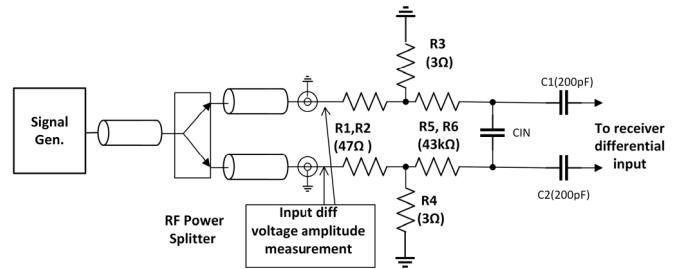
input current with a known amplitude is produced with the input resistors R5 and R6. The capacitance C_{in} then emulates the capacitance of the APD ($\sim$1.5pF). The total input capacitance was evaluated to be $\sim$3.5pF. Since the signal generator provides a continuous sinusoid waveform at the desired frequency, the frequency was swept here from 100kHz to 50MHz and the transimpedance was measured at several specific frequencies.

The measured frequency response is shown in Fig. 13, where the equivalent gain and bandwidth ($-$3dB) are 3.3MΩ and 15MHz, respectively, which match well with the simulations. To confirm the bandwidth result, the bandwidth was also measured with an APD connected to the input to the receiver and the APD was then illuminated with a constant optical power. This illumination produced a dc current in the APD and if the rms value of the shot noise of this current was considerably larger than the equivalent input current noise of the receiver, the frequency response could be recorded as the response of the receiver to this shot noise. The result of this measurement confirmed a bandwidth of 15MHz.

B. Receiver Noise

The receiver noise was measured from the output of the analogue receiver channel with a FFT analysis of the receiver output. Since the receiver noise is critically dependent on the input capacitance, the APD was connected but sheltered from the background illumination. The measured noise spectrum at three APD bias voltages, 0V, 53V and 55V, is shown in Fig. 14. The effect of the APD dark current is clearly seen in the spectrum. The total output voltage noises were $12mV_{rms}$ and $16mV_{rms}$, with bias voltages of 53V and 55V, respectively. The corresponding equivalent input noise currents were $3.6nA_{rms}$, and $4.8nA_{rms}$, respectively. The total equivalent input noise current of the receiver without the APD (but including the preamplifier input equipped with an extra 1.5pF capacitance mimicking the APD capacitance) was found to be $\sim$2.8nA$_{rms}$.

C. Timing Walk Error

A measurement board for the system level tests was constructed which included the designed receiver chip with an APD detector (IAG200, Laser Components), two external timing comparators and a custom-designed CMOS time-to-digital converter (TDC) circuit as described in detail in [31]. Using this approach, the time position of the detected echo could be determined (stop 1) with respect to the transmitted
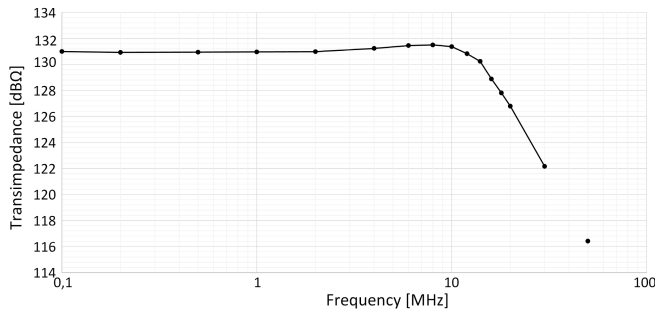
Fig. 13.   Measured frequency response of the receiver channel (the slight peaking is due to the small parallel stray capacitance of resistors R5 and R6).
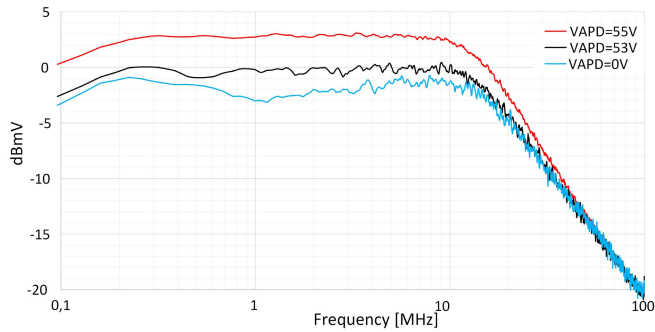

Fig. 14.   Measured noise spectrum at the output of the receiver channel.

laser pulse (start). In addition, the multi-channel TDC allowed one to measure the width (stop3 – stop1) or the rise time (stop2 – stop1) of the timing pulse. A 1550nm laser diode (optical BW ∼20nm) with a stripe width of 50um, pulse peak power of ∼4W and pulse width of 20ns was used as the optical transmitter of the system. The divergences of the transmitter and receiver were 2mrad and 14mrad, respectively. The receiver optics had an effective aperture of ∼20mm in the system tests and were equipped with an optical band-pass filter with a bandwidth of 50nm (FWHM). The measurement configuration is presented in Fig. 15.

The lower and higher threshold levels of the two timing comparators were set at SNR∼5 and SNR∼10, respectively. The two calibration curves produced for timing walk error compensation showed the variation in the pulse width and time interval between the two threshold levels as functions of the input signal strength. For this measurement a reflective target was positioned at a distance of ∼40m from the radar and two variable optical neutral density filters were positioned at the front of the transmitter optics. In this way, the signal strength of the receiver could be adjusted in a controlled manner. To determine the effect of the bias point of the APD, the measurements were carried out at $V_{APD,bias}$ levels of 53V and 55V, at which the APD gains were estimated to be 6.7 and 10, respectively.

The results in Fig. 16 show the dependence of the time position (with respect to the start signal) of the recorded timing signal stop1 on the signal strength given in SNR units at a constant target distance (@40m). It is seen that this uncompensated timing walk error amounts to ∼25ns, which corresponds to a distance of ∼4m. The results also show that
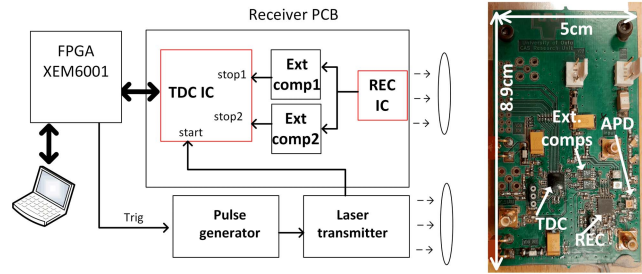

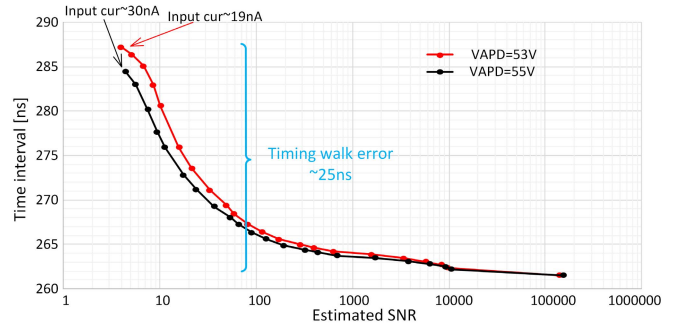Fig. 15.   System test measurement configuration.

Fig. 16.   The dependence of the time position of the stop1 signal as a function of signal strength (i.e. timing walk error). The measurement was done with two V_{APD} bias voltages.
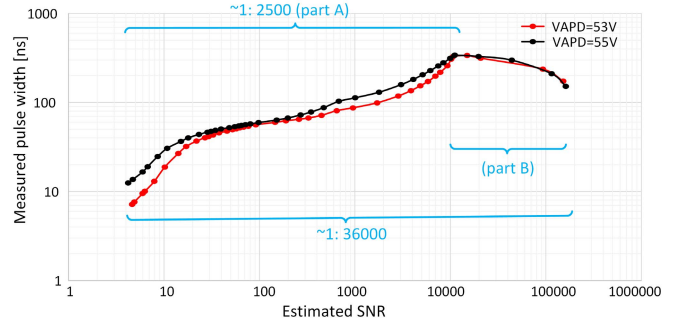

Fig. 17.   The dependence of the timing pulse width on the signal strength. The measurement was done with two V_{APD} bias voltages.

the lower APD bias voltage of 53V gives a higher SNR than does the higher voltage, 55V, as already anticipated above on the basis of the noise calculations.

As suggested above, additional time parameters are measured from the timing pulse in order to compensate for this error. These are the width of the timing pulse at the lower threshold, corresponding to an SNR of ∼5, see Fig. 3, and the time interval required for the timing signal to slew from the lower to the higher threshold, that corresponding to an SNR of ∼10.

The measured dependence of the timing pulse width at the input to the timing comparators on the signal strength is shown in Fig. 17. The total dynamic range of the input signal amplitude in this measurement was ∼1:36 000, and it is seen that in general the pulse width increases with the signal amplitude but starts to shorten above an input signal dynamic range of ∼1: 2500. This shortening can be attributed to the Schottky diodes at the input, which are nevertheless needed to protect the IC and prevent "blocking" of the receiver
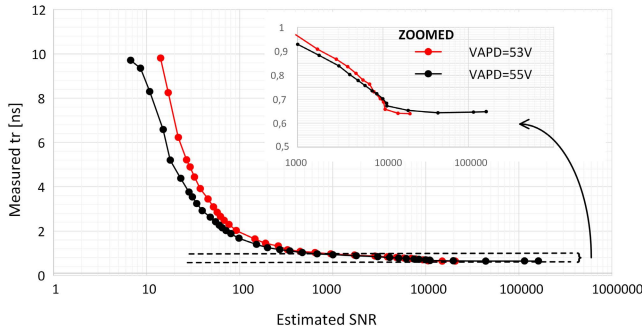
Fig. 18. The dependence of the timing signal slew time between lower and upper threshold on the signal strength.

channel for a long period of time. Thus, if only pulse width compensation were used the unambiguous range for the pulse width measurement-based compensation would not cover the total dynamic range of the signal in this situation. Another timing parameter, the front edge slew rate, is also measured, however, and this opens up a possibility for compensating for the timing walk error within the whole dynamic range, as will be considered next.

The measured dependence of the timing signal front edge slew time on the input signal strength is shown in Fig. 18. As can be seen, this method is operative as soon as the signal amplitude exceeds the higher threshold and works monotonically up to highest signal amplitude values. It is thus possible to compensate for the walk error generated by a dynamic range of 1: 36 000 by means of a combination of pulse width measurement and slew rate measurement. In other words, the measurement of the signal slew time indicates on which side of the maximum pulse width peak seen in Fig. 17 the operation point is and thus enables the correct compensation (from right or left with regard to the pulse width maximum at SNR~10000) to be applied.

Based on the above results, a two-part compensation table was produced to indicate the timing walk error as a function of the timing pulse width. Part A included the timing walk error as a function of the measured pulse width in cases where the compensation was taken from that part of the curve where the pulse width widened monotonously (i.e. from the part with an input dynamic range of ~1: 2500). Part B of the compensation curve applied to the part with a dynamic range of 2500:36000, i.e. where the measured pulse width shortened. As is shown in Fig. 18, the slew rate became saturated at the SNR level where the pulse width started to shorten. As a result, it is part B of the compensation curve that should be used, for example, when the measured slew rate is less than 700ps, the compensation for longer slew times being taken from part A. By using these two time domain parameters, slew time and pulse width, the timing walk error can be compensated for over the whole dynamic range of 1: 36 000. It must be noted, however, that the maximum input signal level is limited by the maximum output power of the laser pulse and not by the compensation method, so that in principle an even wider dynamic range of pulse amplitudes could be compensated for. Thus, time domain data can be used in practical measurements to compensate for the timing error, or even to estimate the strength of the

TABLE II
SYSTEM PARAMETERS FOR LASER PULSE WIDTHS OF 20ns AND 5ns

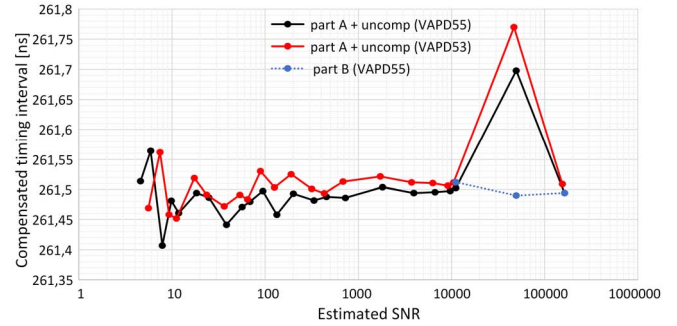| Laser pulse width	20ns	5ns
Uncompensated walk error	25ns	14.4ns
Measured dynamic range	~1:36 000	~1:9400
Min signal in measurements	~19nA	~73nA
Residual walk error	± 150ps (pulse width only)	± 150ps (pulse width only)
Rise time of the output pulse (10%-90%)	15.6ns	9.2ns
Effective transimpedance	2.3MΩ	610kΩ

Fig. 19. Residual timing walk error. Continuous red and black lines: compensated is based on the part A of the compensation curve; blue dashed line: compensated timing results for signal levels SNR>10 000 using part B of the compensation curve.

signal echo. These methods were applied here to record the residual timing walk error. As shown in Fig. 19, this amounts to ~ ±150ps (corresponding to ±2.2cm in distance) over a dynamic range of 1: 36 000 (red and black solid and dashed lines). Compensation for the red and black curves was carried out on the basis of pulse width information only (part A).

Elsewhere, measured timing intervals exceeding an SNR of ~2500 were compensated for by reference to part B of the curve (where the pulse width shortens). As can be seen from Fig. 19, this flattens the bump that occurs at high signal amplitudes, so that the resulting residual timing walk error is ±75ps (corresponding to ±1.1cm) over a dynamic range of 1: 36 000.

The above measurements were then repeated using a laser pulse of length 5ns. The results obtained from the two experiments, as presented in Table II, show that the effective transimpedance was obviously lower with the 5ns pulse length (610kΩ versus 2.3MΩ) as indicated by the bracketed term in the numerator of (6), and thus the minimum detectable signal was also higher (73nA versus 19nA).

The measured timing jitter of the measurement, which indicates the precision of a single shot measurement, is shown in Fig. 20 as a function of the signal strength. In the measurement results shown in Fig. 20, the used laser pulse width was 20ns. As suggested by (3), the jitter improves along with the SNR, so that the measured jitter is ~2.5ns at an SNR of 10. It should also be noted that the jitter can be reduced by applying pulse width measurement-based timing walk error compensation (in this case using the part A and part B compensation curves), i.e. the noise levels at the leading and trailing edges of the timing

TABLE III
PERFORMANCE SUMMARY AND COMPARISON OF RECENTLY PUBLISHED RECEIVERS

	This work	[25] 2020	[23] 2019	[16] 2014	[18] 2020
Technology	0.35 µm CMOS	0.18 µm CMOS	0.35 µm CMOS	0.35 µm CMOS	0.35 µm CMOS
Power consumption	60mW	200mW	180mW	79mW	155mW
Bandwidth	15MHz	280MHz	250MHz	160MHz	230MHz
Input-referred rms noise current	~3nArms C_{total} ~3.5pF C_{pd} ~1.7pF	80nA C_{pd} ~1.2pF	100nA C_{total} ~3pF	19nA C_{pd} ~2.5-5pF	70nA C_{total} ~4pF
Dynamic range Timing walk	1:36 000 +/-75ps	1:5000 +/-30ps	1:40 000 +/-20ps	1:12 000 +/-1.4ns	1:50 000 +/-100ps
Precision	1.7ns @ SNR=10 ~100ps@i$_s$=2uA	62ps @SNR=25	174ps @SNR=13	NA	100ps @ SNR=12
Minimum detectable signal current	19nA @SNR=5	2uA @SNR=25	1uA @SNR=10	63nA @SNR=3	0.6uA @SNR=9
Front end technique	R-TIA	R-TIA	R-TIA	C-TIA	R-TIA
Walk compensation	pulse width+slew time	pulse width+peak detection	pulse width	gain control + delay detection	not needed: front end pulse shaping
System demos: power/length wavelength rec aperture range	4W/20ns 1550 nm 20mm ~330m	NA	12W/3ns 905nm 20mm ~33m	NA/5ns 1550nm NA NA	20W/~3ns 905nm NA NA

pulse correlate to some degree. At higher SNR values the jitter will become saturated at ~100ps. In principle, the timing walk error compensation could be carried out based on slew time measurement only, but in that case the jitter would increase as can be seen from in Fig. 20 c).

D. Transient Recording Mode

When testing the transient operation mode the configuration was as above but a laser pulse with a width of 1ns and SNR varying from 0.5 to 5 was used. The laser pulse was shortened to check the possibility of detecting very short, low intensity laser pulses in the transient mode beyond the intended main operation region. Fig. 21 shows the result recorded at the output from the comparator with a sampling rate of 2.5GSa/s. The results represent averages of one thousand single shots. It is seen that the average of the output signal outside the pulse region is ~1.5V, as it should be with a 3.3V supply voltage, and that there is an equal probability of detecting 0 or 1 for the channel noise. Also, a signal pulse with SNR ~0.5 can easily be detected by averaging 1000 successive shots, since this improves the SNR by a factor of $\sqrt{1000}$ ~30. Note that the channel response is markedly longer than 1ns due to the lower bandwidth of the channel.

E. A Practical Measurement Case

To demonstrate the sensitivity of the receiver as developed here, a transient to a target at a distance of ~330m was recorded from the analogue output buffer with an oscilloscope (1GHz KEYSIGHT MSOX3104T, 2,5GSa/s and a 3.5GHz Agilent 1131A active probe system). The target was a wall of the university building, as shown in Fig. 22, and the set-up was the same as in the earlier measurements, with a laser pulse length of 20ns (peak power ~4W). The transients recorded in a single shot and after the averaging of two successive shots are shown in Fig. 22. The reference level shown with a black line in the Fig. 22, (80mV) corresponds to an SNR of 5. The total transit time is ~2.25μs, which corresponds
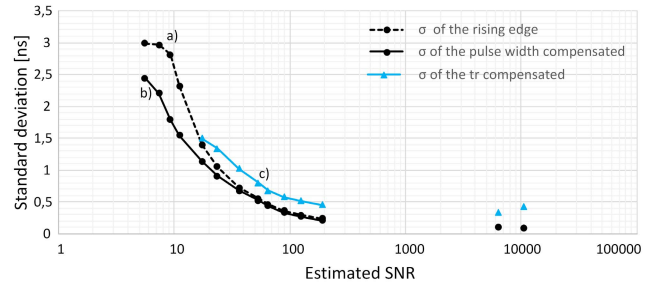

Fig. 20. The dependence of the timing jitter on the measured signal strength for three different timing detection techniques a) detection on the rising edge only, b) detection on the rising edge and pulse width based walk error compensation, c) detection on the rising and rise time measurement based timing walk error compensation.
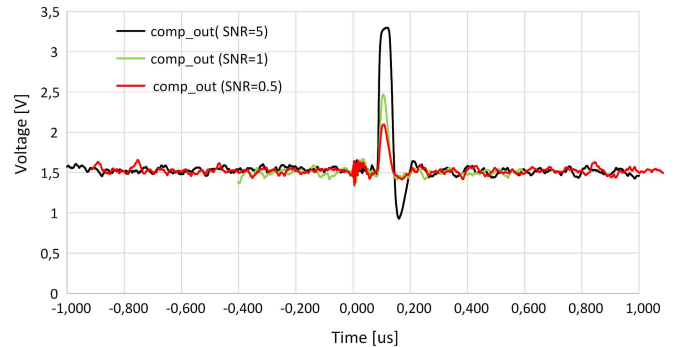

Fig. 21. Output from the receiver channel in the transient recording mode for a laser pulse with a width of 1ns and SNR values of 0.5, 1 and 5 (red, green and black curves). 1000 single shot transients were averaged for each curve.

to a distance of ~330m. The SNR in the single shot was ~9 and could be improved by averaging, as expected. The jitter of the measurement at this point would be 2.5ns and 1.8ns when applying timing walk error compensation. It should be noted that the reference level of SNR = 5 as indicated in the Fig. 22 would be somewhat low for a reliable threshold in a single shot measurement. This is illustrated by the fact that
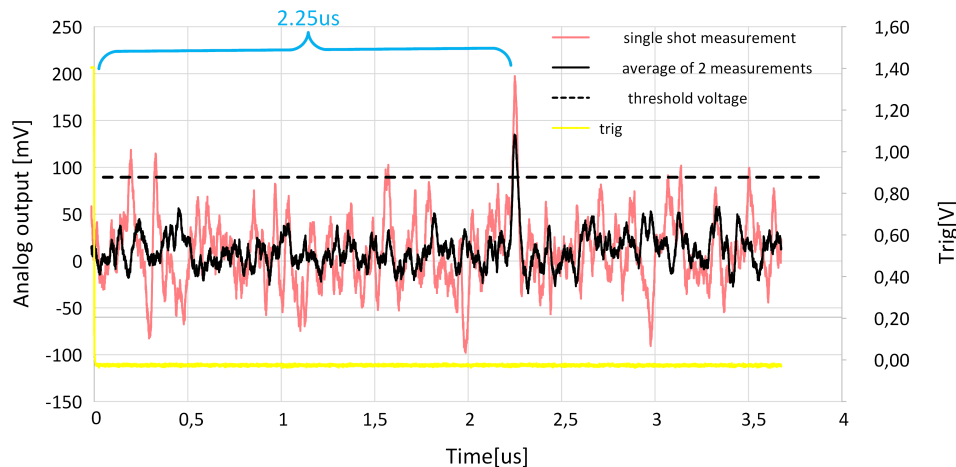
Fig. 22.　Measured signal strength from the wall of a building at a distance of ~330m. A 1550nm laser pulse with a width of 20ns and peak power of ~4W and a receiver aperture of 20mm were used in the measurements.

the transients cross the threshold level at several time points around the position of the target (red curve).

V. Discussion and Conclusion

The low-noise CMOS laser radar receiver channel designed in this work was targeted at 1550nm pulsed time-of-flight laser radar applications using 5ns…20ns laser pulses. The receiver bandwidth of 15MHz was set according to the $\sim 0.15/\Delta T$ rule ($\Delta T = 10$ns), which maximizes the receiver SNR, and thus the sensitivity of the measurement. It has also been shown that even if the receiver bandwidth is markedly lower than that typically used in comparable designs, by utilizing the time domain compensation methods, the timing walk can be reduced to a level of better than $+/-100$ps within a wide dynamic range of 1: 36 000 of received echo amplitudes. The single shot jitter at the limit of detection was in the region of 1.5ns $- 2.5$ns and improved inversely proportionally to the SNR, so that at an SNR of 50 (corresponding to a signal current of ~ 200nA), for example, the single shot jitter was ~ 500ps (corresponding to 7…8cm).

The noise of the receiver (without the contribution of the APD dark current or signal shot noise) was around ~ 3nA$_{rms}$, with a relatively high input capacitance, estimated at ~ 3.5pF. This noise level was much lower than those typically achieved with recently published laser radar receivers [15]–[18], [25]. It was also shown by using the designed receiver in a pulsed TOF laser radar configuration that it allows single shot measurements of distances to non-cooperative targets over a range of several hundred metres with a modest laser power of 4W and a receiver aperture of 20mm. In its transient averaging mode the receiver allows measurements with SNR values below the typical threshold limit, albeit at the cost of increased measurement times.

A comparison of some recent relevant laser radar receiver designs and their main performance parameters is shown in Table III. One distinct feature of the present design is its particularly low input noise level, which is achieved mainly by using a receiver bandwidth optimized for the detection of the laser pulse. In spite of the low bandwidth, high timing accuracy is achieved over a wide dynamic range due to the use of measurements of the slew time of the trailing edge and the width of the timing pulse to compensate for the timing walk error.

References

[1] I. Kaisto, J. Kostamovaara, M. Manninen, and R. Myllyla, "Optical range finder for 1.5–10-m distances," *Appl. Opt.*, vol. 22, no. 20, Oct. 1983, pp. 3258–3264.

[2] J. Kostamovaara, K. E. Maatta, and R. A. Myllylae, "Pulsed time-of-flight laser range-finding techniques for industrial applications," in *Proc. SPIE Conf. Intell. Robot. Syst.*, vol. 1614, Boston, MA, USA, Nov. 1991, pp. 283–295.

[3] A. S. Huntington, G. M. Williams, and A. O. Lee, "Modeling false alarm rate and related characteristics of laser ranging and LIDAR avalanche photodiode photoreceivers," *Opt. Eng.*, vol. 57, no. 7, Jul. 2018, Art. no. 073106.

[4] A. Ullrich and M. Pfennigbauer, "Linear LIDAR versus Geiger-mode LIDAR: Impact on data properties and data quality," *Proc. SPIE*, vol. 9832, May 2016, Art. no. 983204, doi: 10.1117/12.2223586.

[5] J. L. Bufton, "Laser altimetry measurements from aircraft and spacecraft," *Proc. IEEE*, vol. 77, no. 3, pp. 463–477, Mar. 1989.

[6] M. A. Albota et al., "Three-dimensional imaging laser radar with a photon-counting avalanche photodiode array and microchip laser," *Appl. Opt.*, vol. 41, no. 36, pp. 7671–7678, 2002, doi: 10.1364/ao.41.007671.

[7] C. Niclass, "A 100-m range 10-frame/s 340×96-pixel time-of-flight depth sensor in 0.18-μm CMOS," *IEEE J. Solid-State Circuits*, vol. 48, no. 2, pp. 559–572, Dec. 2013.

[8] M. Perenzoni, D. Perenzoni, and D. Stoppa, "A 64×64-pixels digital silicon photomultiplier direct TOF sensor with 100-mphotons/s/pixel background rejection and imaging/altimeter mode with 0.14% precision up to 6 km for spacecraft navigation and landing," *IEEE J. Solid-State Circuits*, vol. 52, no. 1, pp. 151–160, Jan. 2016, doi: 10.1109/jssc.2016.2623635.

[9] D. Bronzi, Y. Zou, F. Villa, S. Tisa, A. Tosi, and F. Zappa, "Automotive three-dimensional vision through a single-photon counting SPAD camera," *IEEE Trans. Intell. Transp. Syst.*, vol. 17, no. 3, pp. 782–795, Mar. 2016, doi: 10.1109/tits.2015.2482601.

[10] J. Kostamovaara, S. S. Jahromi, and P. Keränen, "Temporal and spatial focusing in SPAD-based solid-state pulsed time-of-flight laser range imaging," *Sensors*, vol. 20, no. 21, p. 5973, Oct. 2020, doi: 10.3390/s20215973.

[11] M. Perenzoni, L. Pancheri, and D. Stoppa, "Compact SPAD-based pixel architectures for time-resolved image sensors," *Sensors*, vol. 16, no. 5, p. 745, May 2016, doi: 10.3390/s16050745.

[12] D. G. Fouche, "Detection and false-alarm probabilities for laser radars that use Geiger-mode detectors," *Appl. Opt.*, vol. 42, pp. 5388–5398, Sep. 2003, doi: 10.1364/ao.42.005388.

[13] M. Henriksson, "Detection probabilities for photon-counting avalanche photodiodes applied to a laser radar system," *Appl. Opt.*, vol. 44, pp. 5140–5147, 2005, doi: 10.1364/ao.44.005140.

[14] C. P. Bradley, S. S. Mukherjee, A. D. Reinhardt, P. F. McManamon, A. O. Lee, and V. Dhulla, "3D imaging with 128×128 eye safe InGaAs p-i-n lidar camera," *Proc. SPIE*, vol. 11005, May 2019, Art. no. 1100510, doi: 10.1117/12.2521981.

[15] T.-H. Ngo, C.-H. Kim, Y. J. Kwon, J. S. Ko, D.-B. Kim, and H.-H. Park, "Wideband receiver for a three-dimensional ranging LADAR system," *IEEE Trans. Circuits Syst. I, Reg. Papers*, vol. 60, no. 2, pp. 448–456, Feb. 2013.

[16] H. S. Cho, C. H. Kim, and S. G. Lee, "A high-sensitivity and low-walk error LADAR receiver for military application," *IEEE Trans. Circuits Syst. I, Reg. Paper*, vol. 61, no. 10, pp. 3007–3015, Oct. 2014.

[17] S. Kurtti, J. Nissinen, and J. Kostamovaara, "A wide dynamic range CMOS laser radar receiver with a time-domain walk error compensation scheme," *IEEE Trans. Circuits Syst. I, Reg. Papers*, vol. 64, no. 3, pp. 550–561, Mar. 2017.

[18] A. Baharmast, S. Kurtti, and J. Kostamovaara, "A wide dynamic range laser radar receiver based on input pulse-shaping techniques," *IEEE Trans. Circuits Syst. I, Reg. Papers*, vol. 67, no. 8, pp. 2566–2577, Aug. 2020.

[19] R. G. Smith and S. D. Personick, "Receiver design for optical fiber communication systems," in *Topics in Applied Physics: Semiconductor Devices for Optical Communication*, vol. 39, H. Kressel, Ed. Berlin, Germany: Springer Verlag, 1980, pp. 89–160.

[20] E. Sáckinger, *Broadband Circuits for Optical Fiber Communication*. New York, NY, USA: Wiley 2005.

[21] A. Sharif-Bakhtiar and A. C. Carusone, "A 20 Gb/s CMOS optical receiver with limited-bandwidth front end and local feedback IIR-DFE," *IEEE J. Solid-State Circuits*, vol. 51, no. 11, pp. 2679–2689, Nov. 2016.

[22] M. G. Ahmed *et al.*, "A 12-Gb/s -16.8-dBm OMA sensitivity 23-mW optical receiver in 65-nm CMOS," *IEEE J. Solid-State Circuits*, vol. 53, no. 2, pp. 445–457, Feb. 2018.

[23] S. Kurtti, J.-P. Jansson, and J. Kostamovaara, "A CMOS receiver–TDC chip set for accurate pulsed TOF laser ranging," *IEEE Trans. Instrum. Meas.*, vol. 69, no. 5, pp. 2208–2217, May 2020, doi: 10.1109/TIM.2019.2918372.

[24] J. Nissinen, I. Nissinen, and J. Kostamovaara, "Integrated receiver including both receiver channel and TDC for a pulsed time-of-flight laser rangefinder with cm-level accuracy," *IEEE J. Solid-State Circuits*, vol. 44, no. 5, pp. 1486–1497, May 2009.

[25] X. Wang, R. Ma, D. Li, H. Zheng, M. Liu, and Z. Zhu, "A low walk error analog front-end circuit with intensity compensation for direct ToF LiDAR," *IEEE Trans. Circuits Syst. I, Reg. Papers*, vol. 67, no. 12, pp. 4309–4321, Dec. 2020.

[26] G. M. Williams, "Optimization of eyesafe avalanche photodiode lidar for automobile safety and autonomous navigation systems," *Opt. Eng.*, vol. 56, no. 3, Mar. 2017, Art. no. 031224, doi: 10.1117/1.OE.56.3.031224.

[27] J. Wang and J. Kostamovaara, "Radiometric analysis and simulation of signal power function in a short-range laser radar," *Appl. Opt.*, vol. 33, no. 18, pp. 4069–4076, Jun. 1994.

[28] P. Palojarvi, T. Ruotsalainen, and J. Kostamovaara, "A 250-MHz BiCMOS receiver channel with leading edge timing discriminator for a pulsed time-of-flight laser rangefinder," *IEEE J. Solid-State Circuits*, vol. 40, no. 6, pp. 1341–1349, Jun. 2005.

[29] R. J. van de Plassche and P. Baltus, "An 8-bit 100-MHz full-Nyquist analog-to-digital converter," *IEEE J. Solid-State Circuits*, vol. 23, no. 6, pp. 1334–1344, Dec. 1988.

[30] E. Sackinger, "On the noise optimum of FET broadband transimpedance amplifiers," *IEEE Trans. Circuits Syst. I, Reg. Papers*, vol. 59, no. 12, pp. 2881–2889, Dec. 2012.

[31] J.-P. Jansson, V. Koskinen, A. Mäntyniemi, and J. Kostamovaara, "A multichannel high-precision CMOS time-to-digital converter for laser-scanner-based perception systems," *IEEE Trans. Instrum. Meas.*, vol. 61, no. 9, pp. 2581–2590, Sep. 2012.

Sami Kurtti was born in Kuusamo, Finland, in 1979. He received the M.Sc.Eng. and Dr.Tech. degrees in electrical engineering from the University of Oulu, Finland, in 2004 and 2013, respectively. He was a Research Scientist from 2004 to 2013 and has been a Postdoctoral Researcher with the Circuits and Systems Research Unit, University of Oulu, since 2013. His interests include the development of analog and mixed-signal integrated circuits and structures for pulsed time-of-flight laser rangefinders.

Aram Baharmast (Graduate Student Member, IEEE) received the M.Sc. degree in electronics from Iran University of Science and Technology (IUST), Tehran, Iran, in 2013. Since 2016, he has been a part of the Circuits and Systems Research Unit (CAS), University of Oulu, working as a Ph.D. Researcher, developing integrated circuits for pulsed time-of-flight (TOF) laser rangefinders. In 2021, he joined Nordic Semiconductor as an Analog IC Design Engineer focusing on integrated solutions for power management ICs.

Jussi-Pekka Jansson received the M.Sc. (Tech.) and Dr.Tech. degrees in electrical engineering from the University of Oulu, Oulu, Finland, in 2004 and 2012, respectively. He received an Adjunct Professorship from the University of Oulu in 2017. He has been a University Researcher with the Circuits and Systems Research Unit, University of Oulu, since 2020. His current research interests include high-precision time-to-digital converter (TDC) architectures and applications related to them.

Juha Kostamovaara (Life Senior Member, IEEE) received the Dr. Eng. degree in electrical engineering from the University of Oulu, Oulu, Finland, in 1987. He held the academy professorship position nominated by the Academy of Finland from 2006 to 2011 and then for the second time from 2012 to 2017. He acts as a Professor (Emeritus) in Electronics with the Circuits and Systems Research Unit, University of Oulu. His main research interest is in the development of pulsed time-of-flight devices, circuits, and systems for electronic and optoelectronic measurements.